Quantum States of Molecular Hydrogen and Its Isotopes in Single-Walled Carbon Nanotubes

Tun Lu and Evelyn M. Goldfield*

Department of Chemistry, Wayne State University, Detroit, Michigan 48202

Stephen K. Gray

Chemistry Division, Argonne National Laboratory, Argonne, Illinois 60439

Received: May 8, 2003; In Final Form: September 2, 2003

Quantum mechanical energy levels are computed for the hydrogen molecule and its homonuclear isotopes confined within nanotubes of various sizes and structures. A realistic many-body potential is used to compute the interactions between the atoms of the diatomic and the nanotube carbons. Two translational and two rotational degrees of freedom are treated explicitly. Zero-pressure quantum sieving selectivities are computed from the energy levels. The effects of including both translation and rotation are discussed. The effect of confinement on the ortho/para splitting of hydrogen is also discussed.

I. Introduction

Carbon nanotubes (CNTs) have generated considerable interest recently, in part because of their potential technological uses. In particular, the adsorption of hydrogen on graphite and CNTs has been the focus of much attention largely because of the potential use of CNTs to store hydrogen for use in fuel cells. There have been a number of reports indicating that CNTs can adsorb significant quantities of hydrogen,[1−8] although these results are not free from controversy.[9] Another related potential application of CNTs and other porous materials is as a special type of molecular sieve,[10] a quantum sieve to separate mixtures of molecules that are similar in size and in shape, for example isotope separation. The focus of this paper is on quantum sieving and rotational effects. These calculations, however, are part of a long-range study of the effects of confinement on individual molecules and on reaction dynamics.

Classical molecular sieves separate molecules based on size, shape, or chemical affinity. They cannot be used for isotope separation because isotopes do not differ in these properties, only in their masses. In contrast to a classical sieve, a quantum sieve separates isotopes based upon preferential adsorption of heavier isotopes due to the difference in quantum mechanical energy levels of the atoms or molecules confined in the CNT or other porous material.[11−16]

Quantum sieving was originally proposed by Beenakker and co-workers using a simple model of adsorption of hard spheres in a square-well cylindrical tube.[10] They found high selectivity at 10 K for helium isotopes. Johnson and co-workers have extended these ideas using more realistic models to treat the effects of confinement. They proposed that CNTs could be used to separate isotopes of hydrogen and other light systems.[11−13] The model they used treated the molecule as a spherical object with discrete energy levels in the radial direction perpendicular to the tube axis. They used a one-dimensional potential to compute these levels. Using Grand Canonical Monte Carlo methods, they were able to treat pressure effects.[13] They predicted high selectivity for D_2 and T_2 over H_2 for tubes with diameters about 6 Å at 20 K. They also predict an increase in selectivity with an increase in pressure. Recently, Gordillo et al.[14] have performed Monte Carlo calculations to study isotope effects of hydrogen adsorption within CNTs and in the interstitial channels of bundles of CNTs. They too use a spherically averaged model that did not include rotation. Their calculations predict much more modest selectivity for molecules adsorbed within (5,5) nanotubes.

Hathorn, Sumpter, and Noid[15] proposed that in addition to radial confinement, the hindered molecular rotation of molecules confined in CNTs ought to contribute to quantum sieving. Using a simple semiclassical model of rotation, they computed the selectivity factor for D_2 and T_2 over H_2, as a function of tube diameter. They concluded that for tubes with diameters of 8 Å or less, rotation should contribute significantly to quantum sieving at low temperatures.

In a related study, Trasca et al. studied both spin and isotope selectivity of H_2 adsorbed in the interstitial channels and on the grooves of bundles of CNTs at low pressures.[16] They considered both rotational and translational effects using a 2D harmonic oscillator-rigid rotor model. Thus unlike the present calculation, the effects of rotation and translation were treated as separable. Trasca et al.[16] predicted very large isotope selectivity for D_2 over H_2 in the interstitial channels at low temperatures and pressures, considerably larger than previous predictions for bundles CNTs of similar diameter by Johnson and co-workers.[13]

Our work on quantum sieving is motivated by the work of Johnson and co-workers[11−13]and Hathorn, Sumpter, and Noid.[15] It represents an extension of their ideas to include both rotation and translational degrees of freedom and their coupling using a many-body potential energy surface and rigorous quantum methods. We study the effects of confinement in small single-walled CNTs on molecular hydrogen and its isotopes dynamics. Except for motion along the nanotube axis itself, we explicitly treat all of the motions of the hydrogen relative to the tube: the motion of the H_2 center-of-mass in a plane perpendicular to the tube axis, and rotation about that center-of-mass, resulting in a four-degree-of-freedom problem. These motions correspond

10.1021/jp030601n CCC: $25.00
Published on Web 10/31/2003

TABLE 1: Zero-Point Energies and Quantum Sieving Selectivity at 20 K[a]

nanotube	diameter (Å)	potential minimum, cm^{-1}	ZPE(H_2), cm^{-1}	ZPE(D_2), cm^{-1}	ZPE(T_2), cm^{-1}	$S_0(D_2/H_2)$ at 20 K	$S_0(T_2/H_2)$ at 20 K
(3,6)	6.22	−1540.80	155.03	103.88	82.20	19.99	69.58
(8,0)	6.26	−1475.51	154.23	103.29	81.51	19.71	70.28
(2,8)	7.18	−1173.40	121.32	102.05	91.86	3.13	6.32
(6,6)	8.14	−988.62	150.87	123.87	109.19	5.19	8.51
(10,10)	13.56	−728.50	174.93	142.31	124.37	6.71	20.52

[a] The zero of energy is that of the diatomic at an infinite distance from the nanotube.

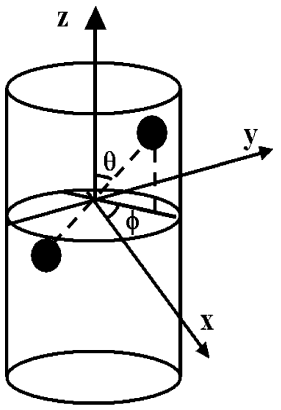

Figure 1. Coordinates used in the 4D calculations.

to two translations and two rotations in the gas phase and give rise to discrete energy levels within the confinement of the CNT and therefore must be treated quantum mechanically. We use a semiempirical many-body Tersoff−Brenner potential[17,18] to compute the hydrogen−carbon interactions. We calculate the energy levels of H_2, D_2, and T_2 in CNTs of various sizes and shapes. Unlike Johnson and co-workers, our potentials are not smoothed and contain the effects of corrugations. In Section II, we present our model and give the necessary theoretical and computational details. In Section III, we present our results, including the ground-state wave functions, quantum sieving selectivity factors, and a discussion of the ortho/para energy splittings as a function of the size and structure of the CNT. Finally, Section IV summarizes our results.

II. Theoretical and Computational Details

A. Model Hamiltonian and Computational Details. The coordinate system for our four-degree-of-freedom model is displayed in Figure 1. In our model, x and y are Cartesian coordinates representing translational motion of the system orthogonal to the nanotube axis; θ is the angle between the molecular bond and the tube axis, z; and the azimuthal angle, ϕ, represents rotation about the z-axis. The molecular center of mass is fixed at a particular value of z in the center of the tube. We fix the bond length of the diatomic in its equilibrium position and we do not treat motions of the atoms in the carbon CNT. The Hamiltonian for this system is given by

$$H = -\frac{\hbar^2}{2M}\left[\frac{\partial^2}{\partial x^2} + \frac{\partial^2}{\partial y^2}\right] - B\left\{\left(\frac{1}{\sin\theta}\right)\frac{\partial}{\partial\theta}(\sin\theta)\frac{\partial}{\partial\theta} + \frac{1}{\sin^2\theta}\frac{\partial^2}{\partial\phi^2}\right\} + V(x,y,\theta,\phi) \quad (2.1)$$

where M is the total mass of the diatomic and B, the rotational constant, is given by $B = \hbar^2/2\mu r_e^2$, where μ is the reduced mass of the molecule and r_e is the equilibrium bond length. The potential includes all interactions between atoms of the diatomic and the carbon atoms of the CNT. The wave function is expanded in a set of real eigenfunctions of the rotational part of the Hamiltonian,

$$\Psi(x,y,\theta,\phi) = \sum_{j=0}^{j_{max}}\sum_{m=0}^{j}\bar{P}_j^m(\cos\theta)(C_j^m(x,y)\cos m\phi + D_j^m(x,y)\sin m\phi) \quad (2.2)$$

where $\bar{P}_j^m$ is a normalized associated Legendre function and C_j^m and D_j^m are expansion coefficients. The Cartesian coordinates, x and y, are represented on evenly spaced grids and a sinc-DVR is used to compute the action of the kinetic energy operator.[19] To compute the action of the potential energy operator, the wave function is transformed from the rotational basis functions to an angular grid, multiplied by the diagonal potential energy, and transformed back to the basis representation. The homonuclear symmetry of the diatomic molecule results in a decoupling of the Hamiltonian matrix into even ($j = 0, 2, ...$) and odd ($j = 1, 3, ...$) blocks.

We computed the energy levels of H_2, D_2, and T_2, even and odd symmetry, for five CNTs of various structures and sizes. The CNTs had diameters ranging from 6.0 to 13.6 Å. The structure of a CNT is determined by the two-integer pair (m, n), which determines the wrapping of the graphene sheet to form the CNT. If $m = n$, the CNT is called an armchair, while if $m = 0$, the CNT is called a zigzag. Otherwise, the CNT is chiral. An excellent discussion of the structure of single-walled CNTs is given by Wildoer et al.[20] We considered two armchair structures (6,6) and (10,10), one zigzag (8,0), and two chiral CNTs (3,6) and (2,8). The diameters of these nanotubes are given in Table 1.

For each CNT, we computed the relevant energy levels and wave functions for H_2, D_2, and T_2 using the ARPACK (Arnoldi package) software library,[21,22] a collection of subroutines designed to solve large-scale eigenvalue problems. For symmetric matrixes, such as we have here, this robust software package uses the implicitly restarted Lanczos method and is similar in spirit (although not quite the same) as applying the Lanczos algorithm along with explicit reorthogonalization within a Krylov subspace.[23] Like the re-orthogonalized Lanczos method, ARPACK is especially useful if one has degenerate and/or nearly degenerate eigenvalues, as we do in this problem, and if one wishes to inspect the actual eigenfunctions.

Short-range interactions between the H atoms and the carbons in the CNT are modeled by using a realistic many-body Tersoff−Brenner potential.[17,18] This potential has been used to describe graphite, diamond, CNTs, and many hydrocarbon complexes and the results are in good agreement with experiments and with quantum chemical calculations.[18,24] It has also been used to model hydrogen atom storage in single-walled CNTs.[25] In our calculation, the Brenner potential describes the repulsion between the hydrogen and the nanotube. The long-distance van der Waals forces between each hydrogen and each carbon atom are computed with use of a 6-12 Lennard-Jones potential. Because we compute interactions between each H

atom and each C atom, our potential is not isotropic. The long-range hydrogen−carbon interactions take effect at H−C distances ≥1.8 Å and are responsible for the H_2−nanotube attractive interactions. Our potential code is modified from Brennermd, a public domain Fortran molecular dynamics program that is included as part of the Fungimol package.[26] The parameters for both the many-body potential and the long-range 6-12 potential were taken from this program. We developed a parallel implementation of the potential that significantly expedited the calculations.

The number of grid points in x and y is determined by the diameter of the nanotube and the grid spacing. For H_2, we use a grid spacing of 0.165 Å for the (3,6) and (8,0) CNTs, and a larger grid spacing of 0.33 Å for the others. The spacings for the heavier D_2 and T_2 isotopes were reduced by factors of $(\sqrt{2})^{-1}$ and $(\sqrt{3})^{-1}$ respectively. The value of j_{max} was taken to be five. The number of grid points for H_2 ranged from 17 in x and in y for the (2,8) and (6,6) nanotubes, to 21 for the (3,6) and (8,0) nanotubes, and to 35 for the (10,10) nanotube. We tested the accuracy of these results using the (3,6) nanotube, using both smaller and larger grid spacings as well as $j_{max} = 11$. Using a grid spacing of 0.165 Å, our results are converged to 0.01 cm^{-1} within 700 cm^{-1} of the ground-state energy. Results for using the larger grid spacings and the smaller j_{max} are converged, for all diatomics, to within 2%. The convergence is much better for the lower energies that play a dominant role in the quantum sieving.

Because we plan to use these results in future studies, we computed many more energy levels than are required to describe quantum sieving at low temperatures. In most of the calculations, we computed all of the bound energy levels; this number ranged from 149 for H_2 in the (3,6) nanotube to 1862 for T_2 in the (2,8) nanotube. ARPACK[21,22] requires specification of a Krylov space size, NCV, and the number of eigenstates desired, NEV. (Memory requirements are proportional to NCV*N, where N is the matrix dimension.) In most of the calculations NCV was two or three times the value of NEV. The total size of the matrixes ranged from $N = 4335$ to 75600. The larger matrixes correspond to the odd states of T_2. To converge 1200 energy levels for the odd T_2 levels of the (6,6) nanotube required 3 days of computing on a single 850-GHz processor of an eight-processor Sunfire 6800 with 8 GB of memory.

B. Partition Functions and Quantum Sieving. The theory of quantum sieving is based upon the idea that due to the difference in their energy levels, heavier isotopes will preferentially bind to the nanotube. To a first approximation, this preference is a result of the zero-point energy differences that can be attributed to the difference in masses.[11−13,15] We can define a low-pressure selectivity factor, $S_0(2/1)$, for isotope 2 over isotope 1, which is the ratio of equilibrium constants for adsorption:

$$S_0(2/1) = \frac{K_2}{K_1} = \frac{Q_{ads,2}}{Q_{free,2}} \frac{Q_{free,1}}{Q_{ads,1}} \tag{2.3}$$

where K_n is the equilibrium constant for adsorption for molecule n, and Q_{ads} and Q_{free} are the corresponding adsorption and free partition functions, respectively. The free partition function is a product of translational and rotational partition functions,

$$Q_{free} = Q_{trans,xy} Q_{rot} \tag{2.4}$$

accounting for two free translational degrees of freedom as well as free molecular rotation. We use a simple classical translational partition function,

$$Q_{trans,xy} = \left(\frac{2\pi m k_b T}{h^2}\right) V^{2/3} \tag{2.5}$$

where V is the volume of the system. We treat the motion along the nanotube axis, z, as free motion so that the translational partition function, $Q_{trans,z}$, is the same in the adsorbed and free species and will cancel out. While this is an approximation, we expect that it is a very good one. The potential varies only a small amount along the tube axis. It is highest at the end of the tube and lowest at the center, where we do our calculation. The typical variation from end to center is only 25−30 cm^{-1}. The translational partition function, $Q_{trans,xy}$, results in a ratio of masses in S_0, and in fact, this ratio inhibits the selectivity of the heavier isotope. Because we are interested in hydrogen at low temperature where the separation between rotational energy levels with respect to k_bT will be large, we treat the rotational partition function quantum mechanically. We assume that the adsorbed molecules maintain a statistical distribution of ortho and para states, as activated carbon has been shown to interconvert the two species.[27] (It is possible to treat the ortho and para states as separate species, but this complicates the computation of S_0 somewhat and we have not done this.) As in Hathorn, Sumpter, and Noid,[15] the rotational partition function is given by

$$Q_{rot} = g_e \sum_{j=even} (2j+1) \exp\{-(B[j(j+1)]/k_bT)\} + g_o \sum_{j=odd} (2j+1) \exp\{-(B[j(j+1)]/k_bT)\} \tag{2.6}$$

where the g_e and g_o are spin-statistical weighting factors: for hydrogen and tritium, with half-integral nuclear spin they are 1 and 3, respectively, and for deuterium, with nuclear spin of one, they are 6 and 3, respectively. We compute Q_{ads} using the discrete energy levels, E_j, obtained from our four-degree-of-freedom quantum mechanical calculation

$$Q_{ads} = g_e \sum_n \exp[-(E_n^e/k_bT)] + g_o \sum_n \exp[-(E_n^o/k_bT)] \tag{2.7}$$

In eq 2.7, the first and second terms represent energies computed including only the even rotational and odd rotational basis states, respectively.

III. Results

A. Wave Functions and Potentials. In Figure 2, we illustrate our model by showing the hydrogen within the (3,6) nanotube. The nanotube diameters are presented in Table 1. We compute a reduced probability density in x and y by averaging the square of the wave function over the angular coordinates. The reduced probability densities of the ground state for each CNT are shown in Figure 3. These may be grouped into three types. For the smaller CNTs, i.e., (3,6) and (8,0), the system is confined to the center of the nanotube, whereas for larger CNTs, the molecule prefers to be closer to the tube wall. A two-dimensional harmonic oscillator might provide a simple model to qualitatively describe the two-dimensional (2D) confinement in the smaller tubes. A qualitative description of one-dimensional confinement (1D) in the larger tubes, however, could be given by a particle-in-a-ring. The transition from 1D to 2D confinement with decreasing tube diameter was also seen by Johnson and co-workers.[12] The most interesting probability density, however, is that for the (2,8) nanotube, which exhibits considerable structure (but is indeed nodeless as required). One-dimensional cuts of the potential shown in Figure 4 provide

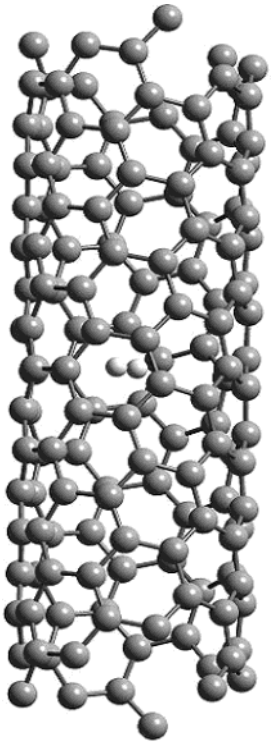

Figure 2. View of H_2 in the center of the (3,6) nanotube.

some explanation of these density plots. Tubes with large diameters exhibit double well potentials with the minima away from the center of the nanotube. As the diameter decreases, these wells move closer together until they finally merge into one well for the smallest CNTs. The (2,8) nanotube, an intermediate case, has two very shallow wells near the center of the tube; this structure is reflected in the ground state wave function. The asymmetric character of the chiral (2,8) nanotube is reflected in the orientation of the lobes of the wave function. The orientation of these lobes will change continuously along the nanotube axis. Note that as the nanotube diameter decreases, the potential wells become flatter, their minima move close together, and the barriers between them are reduced. Finally for the (3,6) and (8,0) CNTs, the wells merge to give rise to a potential that is quite flat at the minimum.

In Figure 5, we show cuts of the potential for the (3,6) and (6,6) nanotubes as a function of the polar angle for rotation, θ. In this plot, the potential is averaged over the azimuthal rotational coordinate, ϕ. The molecular center-of-mass is fixed at the global minimum value, which is at the center of the nanotube for (3,6) and away from the center and about 0.28 Å closer to the wall for (6,6). In both cases the molecule prefers to be aligned parallel to the *z*-axis. The barriers to rotation are largely a function of the proximity to the wall. Thus, the rotational barriers for the (3,6) nanotube are rather small at $\sim$20 cm^{-1}, while those for the (6,6) nanotube are much higher at $\sim$140 cm^{-1}. For a given nanotube, the barriers to rotation with respect to the azimuthal angle, ϕ, are smaller than those with respect to θ and we do not show them.

B. Quantum Sieving Selectivity Factors. We plot the selectivity factors $S_0(D_2/H_2)$ and $S_0(T_2/H_2)$ for the (3,6) and (6,6) CNTs as a function of temperature in Figure 6. We emphasize that these results are valid only in the low-pressure limit. It is obvious from these plots that significant selectivity occurs only at very low temperature. In Table 1, we give S_0 at 20 K for each of the CNTs we computed, along with the nanotube diameter, the minimum energy, and zero point energies for each of the diatomics. Our results at 20 K for the smaller CNTs are considerably smaller than those for Johnson and co-workers,[11,12] in particular our (3,6) and (2,8) results. We believe that the main reason for this is due to the difference in potentials that we use. For example, the Crowell−Brown potential[28] used by Johnson and co-workers does not have the double-well structure

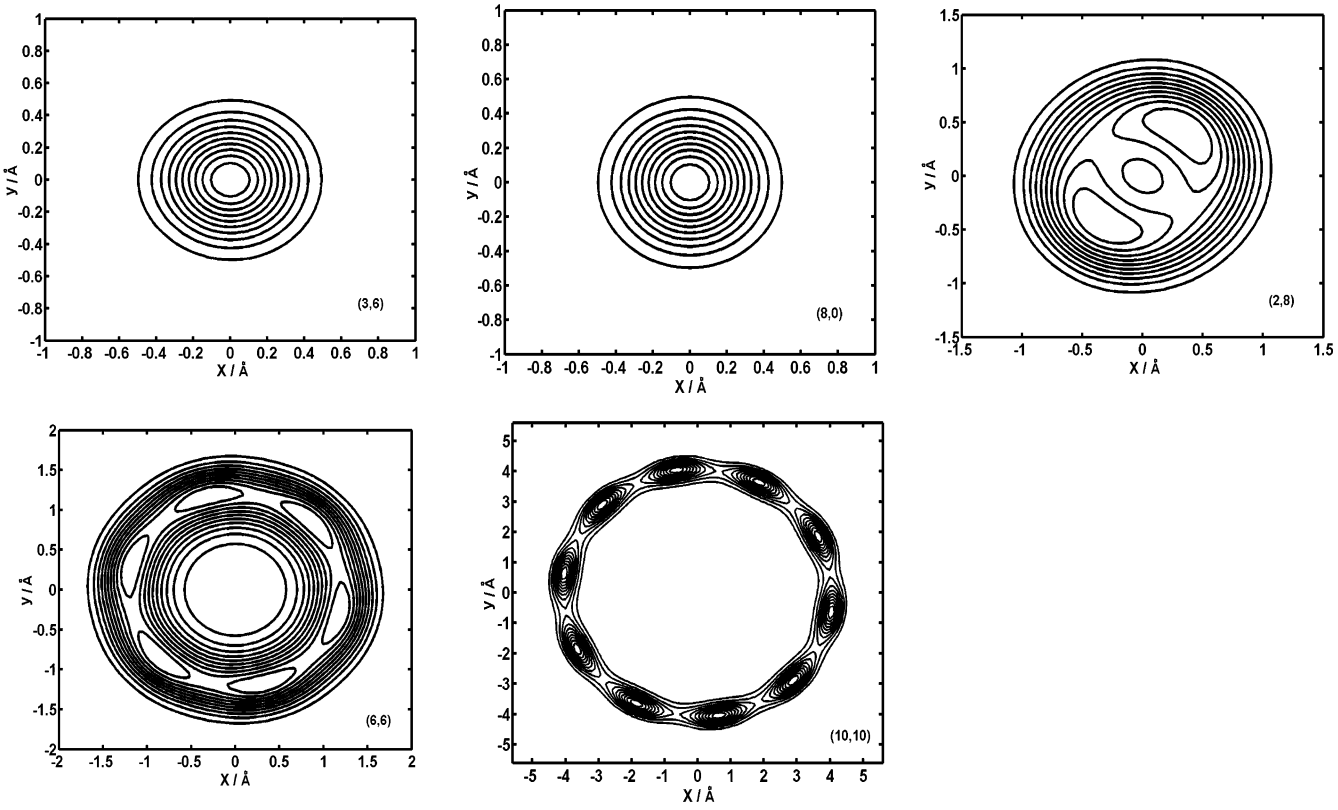

Figure 3. Reduced density plots of the ground state for the (3,6), (8,0), (2,8), (6,6), and (10,10) nanotubes.

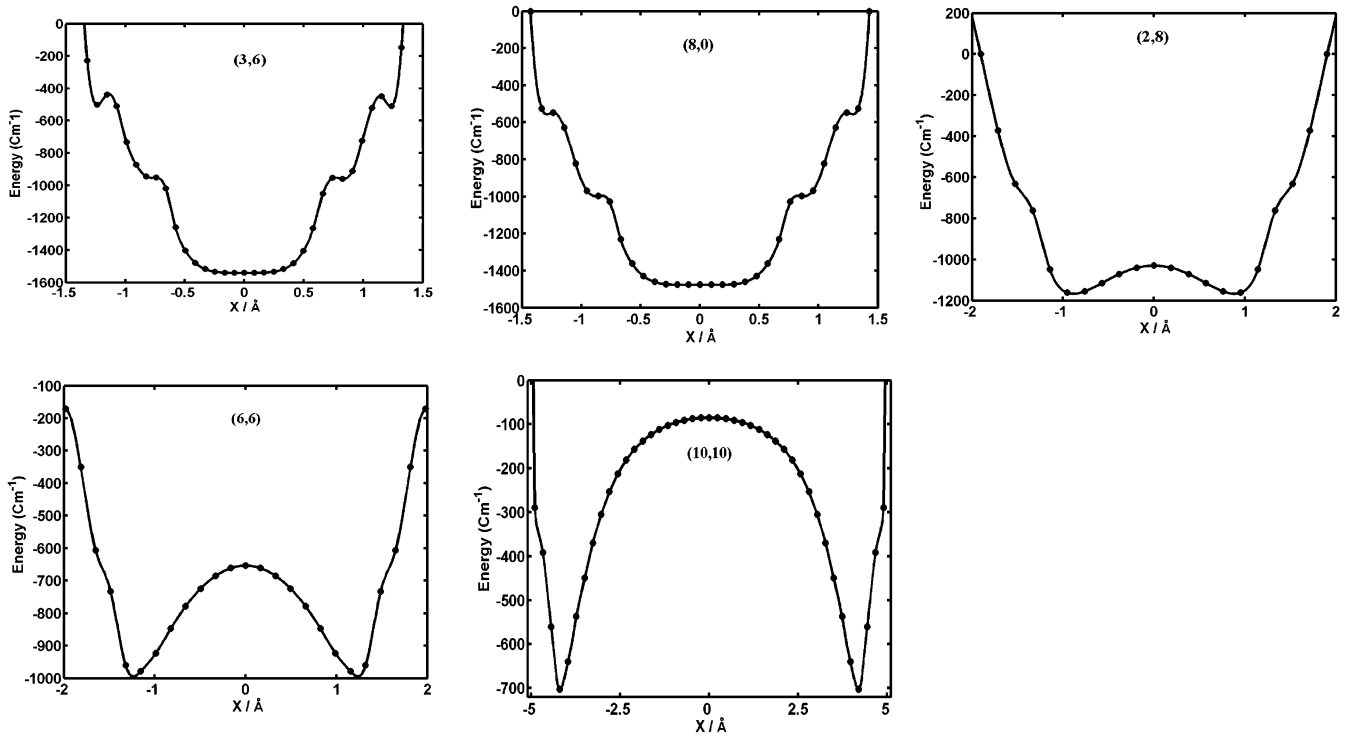

Figure 4. One-dimensional cuts of the potential energy surface as a function of the x coordinate, with $y = 0$, minimized with respect to θ and ϕ.

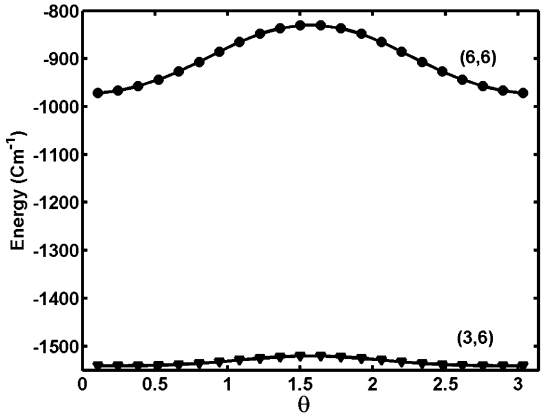

Figure 5. Cuts of the potential energy surface as a function of the polar rotational coordinate, θ, for the (3,6) and (6,6) nanotubes.

for the (2,8) nanotube and appears to be less flat for the smaller nanotubes. The results of Gordillo et al.[14] are more consistent with ours. At 20 K, they predict that for a (5,5) nanotube $S_0(T_2/H_2) = 22.8$ and $S_0(D_2/H_2) = 13.4$.[14,16] The diameter of a (5,5) nanotube, 6.6 Å, is only slightly larger than the diameter of the (3,6) and (8,0) nanotubes. Our results indicate that temperatures less than 20 K are required to see enormous quantum sieving effects, but that modest yet perhaps relevant effects may be seen at higher temperatures. The magnitude of the quantum sieving effects is primarily a function of the diameter, but it is not a monotonic function. The very large effects are seen for very smallest nanotubes, (3,6) and (8,0), where the molecule has 2D confinement in the center of the nanotube. For larger CNTs with double well potentials in x and y and 1D confinement, the quantum sieving selectivity in fact decreases as the diameter decreases. The lowest selectivity occurs for the (2,8) nanotube, which is near the transition between 1D and 2D confinement. This phenomenon is a function of the decrease in the steepness of the potential as the nanotube diameter decreases (see Figure 4). Johnson and co-workers also

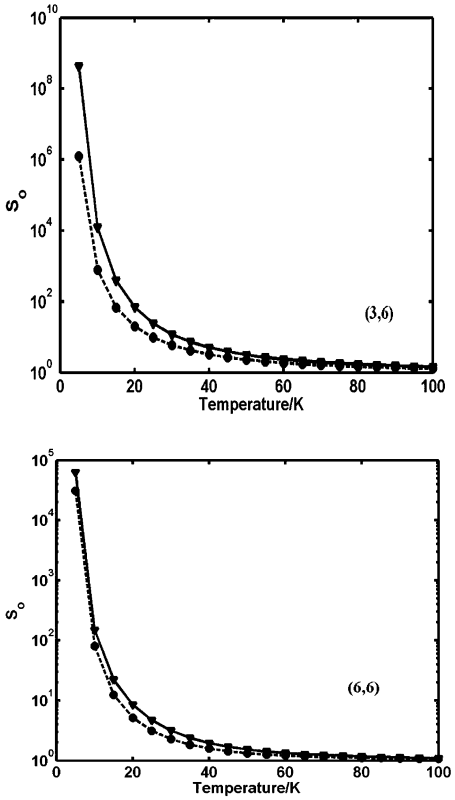

Figure 6. Quantum sieving selectivity, S_0, as a function of temperature for the (3,6) and (6,6) nanotubes: $S_0(D_2/H_2)$, dashed line and circles; $S_0(T_2/H_2)$, solid line and triangles.

see that the lowest selectivity occurs at the transition between 1D and 2D confinement, although in their model the (2,8) CNT exhibits 2D confinement and hence has a higher selectivity than the (6,6) CNT.[12]

Hathorn, Sumpter, and Noid[15] also see significant selectivity factors only for CNTs with diameters near 6.0 Å and at

TABLE 2: Energy Separation of the Lowest Even and Odd Symmetry States

nanotube	ΔE, cm^{-1}
(3,6)	98
(8,0)	96
(2,8)	116
(6,6)	110
(10,10)	108
free	122

temperatures less than 20 K. Unfortunately, single-walled CNTs with diameters less than 7.0 Å are currently difficult to synthesize, although there are recent reports of synthesis of a 5 Å CNT.[29,30] Additionally, the factors of 3−20 seen for larger CNTs at 20 K may also be significant. It is possible that strong quantum sieving effects could also be observed in the interstitial channels of bundles of larger CNTs as suggested by Johnson and co-workers.[13] The work of Trasca et al.[16] supports this suggestion. The interstitial channels have diameters on the order of 6 Å, thus resulting in 2D confinement and hindered rotation.

Our results for the H_2 confined within larger nanotubes are similar to those found in previous studies. However, by using a different many-body potential with corrugations, including rotation−translational couplings, and employing rigorous quantum state calculations, we have solidified the general conclusions of this earlier work.

The zero-point energies (ZPE) for each nanotube are presented in Table 1. For the two smallest, the isotope effect on the ZPE is roughly what one would expect for a two-dimensional harmonic oscillator where the frequency varies inversely as the square root of the mass. A simple harmonic model, however, does not predict the ZPEs of the diatomics in the larger nanotubes.

C. Hindered Rotation of H_2 and Its Isotopes in Single-Walled CNTs. As noted above and shown in Figure 5, cuts of the potential energy surface exhibit barriers to rotation, particularly for rotation about an axis orthogonal to the nanotube axis. The molecule prefers to orient parallel to this axis and to avoid being perpendicular to it. One way to measure the overall effects of hindered rotation is to look at the ortho/para separation, which in our case is the difference in energy between the lowest even and lowest odd energy levels. Brown et al.[31] measured the $j = 0 \rightarrow 1$ transition of hydrogen physisorbed onto the **exterior** surface of CNTs and concluded that the CNT−hydrogen interaction provided only a small barrier to rotation. We have computed the ortho/para separations for hydrogen adsorbed in the interior of CNTs. These results are displayed in Table 2. The magnitude of the ortho/para energy splitting is a function of the diameter of the tube and its structure. The smallest nanotubes give rise to the largest deviations from the free rotor result, but the intermediate (2,8) nanotube is closest to the free rotor splitting. One may wonder why the largest decreases occur for the (3,6) and (8,0) CNTs, given that the rotational barriers were much higher in the larger (6,6) and (10,10) tubes. The answer, in part, is that this splitting is a function not only of the rotational barriers, but also of the translational/rotational coupling. We examined reduced density plots such as those shown in Figure 3 for the lowest odd-j states for the (3,6) and (10,10) CNTs (not shown). The odd-j density for the (10,10) nanotube is nearly identical with the one for the ground state. The situation is quite different in the case of the (3,6) nanotube; however, the density of the lowest odd-j state is quite different from that of the (3,6) ground state: less compact and more structured.

To understand the separate effects of hindered translation and hindered rotation on quantum sieving, we also performed two types of 2D calculations on the (3,6) nanotube. In one of these we used only the translational coordinates and averaged the potential over the angular coordinates. The other 2D calculation was used to study the effects of rotation. We fixed the molecular center-of-mass at various positions along the x-axis and computed the energy levels using only the angular coordinates, θ and ϕ. The effects of including rotation on quantum sieving are not large but significant. For the (3,6) nanotube, using only the translational degrees of freedom, we obtain 78% of the 4D result for $S_0(D_2/H_2)$ and 64% of the 4D result for $S_0(T_2/H_2)$. The increases in ZPE in the full 4D calculations over the translational 2D calculation are somewhat modest: 7.4, 4.1, and 2.5 cm^{-1} for H_2, D_2, and T_2, respectively. Nevertheless, the differential increases for the three diatomics coupled with the effects of translation/rotation coupling on the individual energy levels lead to these enhancements. The energy levels computed for the 2d rotational calculations shed light on this coupling. At the center of the nanotube, the molecule behaves almost as if it were a free rotor with almost no ZPE and all of the free rotor degeneracies quite discernible. The situation is quite different, however, if its center-of-mass is moved 0.5 Å from the center along the x-axis. There the ZPE is very large (194 cm^{-1} for H_2) and the degeneracies are lifted. In the case of 2D confinement, therefore, the effects of rotation are clearly most pronounced on those parts of the wave function that are furthest from the center of the nanotube. The fact that the bulk of the selectivity may be accounted for by translation alone suggests that the separation of translational and rotational degrees of freedom in the computation of the partition functions, as suggested by Hathorn, Sumpter, and Noid,[15] may be a valid approximation. This idea, however, is countered somewhat by the evidence for strong rotational/translational coupling that occurs in the smaller CNTs.

IV. Conclusions

We have computed the low-pressure quantum sieving selectivity factors, S_0, for five CNTs of different shapes ranging in diameter from 6.2 to 13.6 Å. We find S_0 is very large only for CNTs with diameters near 6 and at temperatures below 20 K, but that more modest selectivity occurs for larger tubes at higher temperatures. We found that S_0 is primarily a function of the nanotube diameter and not its shape, but that the function is not monotonic. S_0 decreases with tube diameter until the transition between 1D and 2D confinement is reached, after which it increases significantly. In this respect, our results are consistent with the results of Johnson and co-workers,[11,12] although they see higher selectivity for small CNTs. The selectivity is a strong function of the shape of the potential energy surface. Experimental verification of the theoretical predictions of strong quantum sieving effects for hydrogen isotope separation is a necessary first step in determining whether this phenomenon has potential technological value. It may be that the interstitial channels of bundles of larger CNTs provide the most practical means of demonstrating the quantum sieving effect. It would be interesting to see if the large selectivity effects obtained by Trasca et al.[16] are a result of the special arrangement of the carbon atoms in the interstitial as they suggest or rather a function of their interaction potential.

We also calculated the ortho/para energy separations for H_2. The greatest deviations from the free energy value are found for the smallest nanotubes. The smallest deviation, however, occurs for the (2,8) nanotube, near the transition between 1D and 2D confinement, echoing the trend we see for S_0. It is interesting to speculate that this transition will be fundamental

for other properties of CNTs, in particular their influence on chemical reactions. We see a modest but significant effect of molecular rotation on the quantum sieving selectivity.

The equilibrium constants for adsorption of H_2 and its isotopes in a CNT are also obviously of interest and can be computed from the partition functions. These have been discussed in detail elsewhere.[32] Here we will only comment that, as expected, the smaller tubes bind hydrogen more strongly than the larger tubes. Future work will focus primarily on reactivity in carbon nanotubes and the effects of confinement on chemical reaction rates. We are currently studying hydrogen transfer reactions in CNTs.

Acknowledgment. E.M.G. acknowledges support from DOE (Grant No. DE-FG02-01ER15212). S.K.G. acknowledges support from the Office of Basic Energy Sciences, Division of Chemical Sciences, Geosciences and Biosciences, U.S. Department of Energy, under Contract No. W-31-109-ENG-38.

References and Notes

(1) Darkrim, F.; Vermesse, J.; Malbrunot, P.; Levesque, D. *J. Chem. Phys.* **1999**, *110*, 4020.

(2) Gordon, P. A.; Saeger, P. B. *Ind. Eng. Chem. Res.* **1999**, *38*, 4647.

(3) Simonyan, V. V.; Diep, P.; Johnson, J. K. *J. Chem. Phys.* **1999**, *111*, 9778.

(4) Ye, Y.; Ahn, C. C.; Witham, C.; Fultz, B.; Liu, J.; Rinzler, A. G.; Colbert, D.; Smith, K. A.; Smalley, R. E. *Appl. Phys. Lett.* **1999**, *74*, 2307.

(5) Bauschlicher, C. W. *Chem. Phys. Lett.* **2000**, *322*, 237.

(6) Williams, K. A.; Eklund, P. C. *Chem. Phys. Lett.* **2000**, *320*, 352.

(7) Lee, S. M.; An, K. H.; Lee, Y. H.; Seifert, G.; Frauenheim, T. *J. Am. Chem. Soc.* **2001**, *123*, 5059.

(8) Cheng, H. M.; Yang, Q. H.; Liu, C. *Carbon* **2001**, *39*, 1447.

(9) Yang, R. T. *Carbon* **2000**, *38*, 623.

(10) Beenakker, J. J. M.; Borman, V. D.; Krylov, S. Y. *Chem. Phys. Lett.* **1995**, *232*, 379.

(11) Wang, Q. Y.; Challa, S. R.; Sholl, D. S.; Johnson, J. K. *Phys. Rev. Lett.* **1999**, *82*, 956.

(12) Challa, S. R.; Sholl, D. S.; Johnson, J. K. *Phys. Rev. B* **2001**, *63*, 245419.

(13) Challa, S. R.; Sholl, D. S.; Johnson, J. K. *J. Chem. Phys.* **2002**, *116*, 814.

(14) Gordillo, M. C.; Boronat, J.; Casulleras, J. *Phys. Rev. B* **2002**, *65*, art. no.

(15) Hathorn, B. C.; Sumpter, B. G.; Noid, D. W. *Phys. Rev. A* **2001**, *64*, 22903.

(16) Trasca, R. A.; Kostov, M. K.; Cole, M. W. *Phys. Rev. B* **2003**, *67*, art. no.

(17) Tersoff, J. *Phys. Rev. Lett.* **1988**, *61*, 2879.

(18) Brenner, D. W. *Phys. Rev. B* **1990**, *42*, 9458.

(19) Colbert, D. T.; Miller, W. H. *J. Chem. Phys.* **1992**, *96*, 1982.

(20) Wildoer, J. W. G.; Venema, L. C.; Rinzler, A. G.; Smalley, R. E.; Dekker, C. *Nature* **1998**, *391*, 59.

(21) Lehoucq, R. B.; Sorensen, D. C.; Yang, C. http://www.caam.rice.edu/software/ARPACK.

(22) Lehoucq, R. B.; Sorensen, D. C.; Yang, C. *ARPACK Users' Guide: Solution of Large-Scale Eigenvalue Problems with Implicitly Restarted Arnoldi Methods*; SIAM, 1998.

(23) Golub, G. H.; van Loan, C. F. *Matrix Computations*, 3rd ed.; Johns Hopkins University Press: Baltimore, MD, 1996.

(24) Brenner, D. W. *Carbon* **1990**, *28*, 769.

(25) Ma, Y. C.; Xia, Y. Y.; Zhao, M. W.; Wang, R. J.; Mei, L. M. *Phys. Rev. B* **2001**, *63*, 115422.

(26) Freeman, T. http://www.fungible.com/fungimol.

(27) Davidson, N. *Statistical Mechanics*; McGraw-Hill: New York, 1962.

(28) Crowell, A. D.; Brown, J. S. *Surf. Sci.* **1982**, *123*, 296.

(29) Peng, L. M.; Zhang, Z. L.; Xue, Z. Q.; Wu, Q. D.; Gu, Z. N.; Pettifor, D. G. *Phys. Rev. Lett.* **2000**, *85*, 3249.

(30) Sun, L. F.; Xie, S. S.; Liu, W.; Zhou, W. Y.; Liu, Z. Q.; Tang, D. S.; Wang, G.; Qian, L. X. *Nature* **2000**, *403*, 384.

(31) Brown, C. M.; Yildirim, T.; Neumann, D. A.; Heben, M. J.; Gennett, T.; Dillon, A. C.; Alleman, J. L.; Fischer, J. E. *Chem. Phys. Lett.* **2000**, *329*, 311.

(32) Lu, T.; Goldfield, E. M.; Gray, S. K. *J. Theor. Comput. Chem.* In press.